General IIR Optical Filter Design for WDM Applications Using All-Pass Filters

C. K. Madsen

***Abstract*—A general design algorithm is presented for infinite impulse response (IIR) bandpass and arbitrary magnitude response filters that use optical all-pass filters as building blocks. Examples are given for an IIR multichannel frequency selector, an amplifier gain equalizer, a linear square-magnitude response, and a multi-level response. Major advantages are the efficiency of the IIR filter compared to finite impulse response (FIR) filters, the simplicity of the optical architecture, and its tolerance for loss. A reduced set of unique operating states is discussed for implementing a reconfigurable multichannel selection filter.**

***Index Terms*—All-pass filters, bandpass filters, optical waveguide filters.**

I. Introduction

OPTICAL filters are an enabling technology for dense wavelength-division-multiplexed (DWDM) systems for performing channel (de)multiplexing, add–drop, spectral monitoring, gain equalization, and dispersion compensation. As the channel spacing decreases, the bitrates increase, and point-to-point systems evolve into networks, more filters and filters with more ideal characteristics will be required. In this paper, we discuss infinite impulse response (IIR) filters that can be made quite compact and require significantly fewer stages than comparable finite impulse response (FIR) filters. The IIR architecture is based on decomposing the desired filter response into a sum (or difference) of two all-pass filters. The filter responses are periodic, which is advantageous for WDM systems with many channels since the same filter can be used in different bands [1]. The period is called the free spectral range (FSR). Previous work showed that single-passband (per FSR) elliptic, Chebyshev and Butterworth designs can be implemented using optical all-pass filters in a Mach–Zehnder interferometer (MZI) [2]. In this paper, the design algorithm is generalized so that any magnitude response can be approximated with such an architecture. In particular, the need to have a symmetric magnitude response is overcome.

In Section II, the general design algorithm is presented. An IIR multichannel frequency selector is developed in Section III, and the impact of loss and variations on the filter parameters is investigated. Then, we shift the focus from designing bandpass filters to approximating an arbitrary magnitude response. Examples are given in Section IV for a gain equalization filter and a filter with a linear power response, which may be useful for frequency discrimination or modulation. Finally, a special case of the architecture where one arm is a delay line is discussed in Section V. Examples are presented for a notch filter and a multilevel filter response.

Manuscript received August 11, 1999; revised February 16, 2000.

The author is with the Bell Laboratories, Lucent Technologies, Murray Hill, NJ 07974 USA.

Publisher Item Identifier S 0733-8724(00)05076-3.

II. General Design Algorithm

We are interested in IIR filters with power complementary frequency responses $H_s(\omega)$ and $H_d(\omega)$ that can be decomposed into the sum or difference of two all-pass filters, $A_1(\omega)$ and $A_2(\omega)$, as shown in Fig. 1(a) for a discrete time filter [3]. These filters have a very simple optical implementation as shown in Fig. 1(b)–(d) [2]. The conditions on $H_s(\omega)$ and $H_d(\omega)$ for such a decomposition to exist are derived as part of the synthesis algorithm in this section. To establish the mathematical relationships between the various frequency responses and filter parameters, we begin by discussing discrete time and optical all-pass filters and their Z transforms.

All-pass filters consist of a single input and output with one or more feedback paths. Basic single-stage optical all-pass filters are shown in Fig. 2 [4]. Traveling wave (ring resonators) or standing wave (Gires-Tournois interferometer [5]) feedback paths are used to implement the optical all-pass filters. Power splitters such as directional couplers, multimode interference couplers [6], or reflectors determine the degree of coupling to the feedback path. Tunable all-pass filters, requiring two phase shifters per stage, were demonstrated using a MZI to replace the single coupler of the basic ring design [7]. Reflection-based tunable all-pass filters using microelectromechanical (MEMS) technology have also been demonstrated [8], whereby the partial reflectance is voltage controlled and the cavity phase is temperature controlled. More general all-pass filter architectures are discussed in [9]. For wideband applications, the wavelength dependence of the coupling ratios must be considered. Since there are many ways to reduce the wavelength dependence in practice, we shall assume wavelength-independent coupling for simplicity.

To describe an all-pass filter mathematically, it is convenient to define a nominal feedback path delay, called the unit delay T, which is related to the nominal feedback path length L and group index n_g by $T = n_g L/c$. The unit delay has a frequency response $e^{-j\omega T}$ where ω is the optical radian frequency. By substituting $z^{-1} = e^{-j\omega T}$, we obtain a Z transform description of the optical filter. The Z transform notation allows us to describe a linear, time-invariant filter's transfer function as a ratio of two polynomials in z. The roots of the numerator (z_n) are called the zeros, and the roots of the denominator (p_n) are the poles. The frequency response is found by evaluating the transfer function

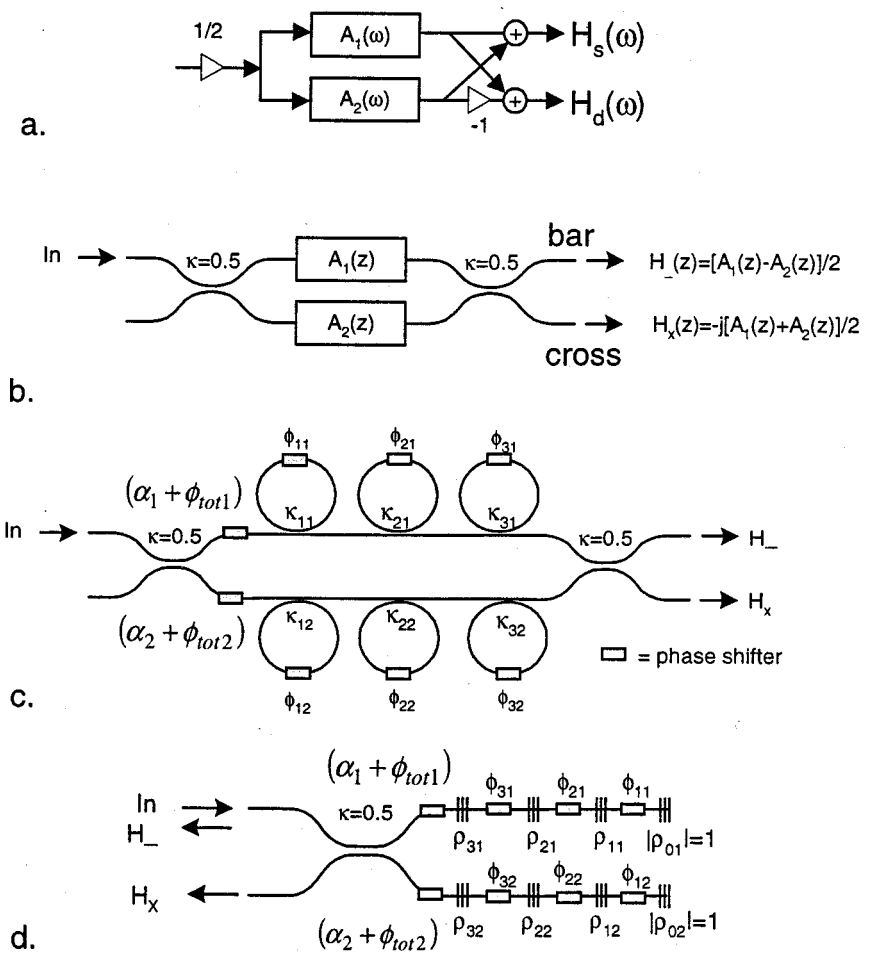

Fig. 1. A general bandpass filter architecture using all-pass filter decomposition in the (a) discrete time and (b) optical domain. A specific sixth-order architecture implemented with (c) a cascade of single-stage ring resonators in each MZI arm and (d) three coupled cavities is depicted. Only half the phase is required by each phase shifter in (d) compared to (c) since the light makes a double pass through each one.

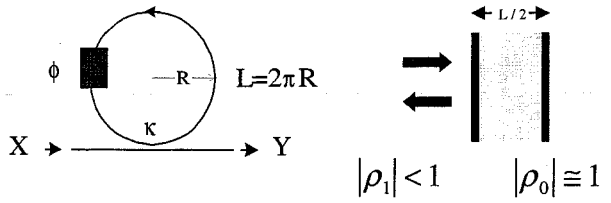

Fig. 2. Basic single-stage optical all-pass filters.

at $z = e^{j\omega T}$. The frequency response is periodic with a period given by FSR = 1/T. A discrete time all-pass filter has a single-stage transfer function given by

$$A(z) \equiv \frac{Y(z)}{X(z)} = \frac{\rho e^{-j\varphi} - z^{-1}}{1 - \rho e^{+j\varphi} z^{-1}} = \frac{D^R(z)}{D(z)}. \tag{1}$$

The superscript R denotes the reverse polynomial, defined by $D^R(z) = z^{-N} D^*(z^{*-1})$ for an Nth-order polynomial $D(z)$. A reverse polynomial is obtained by reversing and conjugating the coefficients of the "forward" polynomial. The magnitudes are the same, i.e., $|D(e^{j\omega})| = |D^R(e^{j\omega})|$, but the phases are different. Note that $|A(e^{j\omega})| = 1$, so the filter passes all frequencies. An optical all-pass filter has the following transfer function for a single stage [4], [10]:

$$A(z) \equiv \frac{Y(z)}{X(z)} = \frac{\rho - e^{+j\phi} z^{-1}}{1 - \rho e^{+j\phi} z^{-1}} = e^{+j\phi} \frac{D^R(z)}{D(z)}. \tag{2}$$

Note the extra phase term not associated with discrete time all-pass filters. There are two degrees of freedom for each stage, ρ and ϕ. They are related to the splitting ratio κ or partial reflectance $\rho = \sqrt{1-\kappa}$ and feedback path phase $\phi \equiv (2\pi/\lambda)\Delta(nL)$ where $\Delta(nL)$ is the deviation of the optical feedback path length from $n_g L$. To model the impact of loss on the response, one simply substitutes γz^{-1} for z^{-1} where the loss for one pass around the feedback path is given

by $-10\log_{10}\gamma^2$ in dB. The phase and group delay response of a single-stage all-pass filter are given by

$$\Phi(\omega)=\tan^{-1}\left\{\frac{(1-\rho^2)\sin(\omega T-\phi)}{2\rho-(1+\rho^2)\cos(\omega T-\phi)}\right\} \quad (3)$$

$$\tau(\omega)=-\frac{d\Phi(\omega)}{d\omega}=\frac{(1-\rho^2)}{1+\rho^2-2\rho\cos(\omega T-\phi)}T. \quad (4)$$

On-resonance, $\omega T=\phi+2\pi m$ where m is an integer, and the group delay is a maximum with a value $\tau_{\max}=(1+\rho)/(1-\rho)T$. Off-resonane, $\omega T=\phi+\pi(2m+1)$, and the group delay has a minimum value of $\tau_{\min}=(1-\rho)/(1+\rho)T$.

We now describe the discrete time transfer function for Fig. 1(a). The output transfer functions are defined by

$$H_s(z)\equiv\frac{N_s(z)}{D(z)} \quad \text{and} \quad H_d(z)\equiv\frac{N_d(z)}{D(z)} \quad (5)$$

where the subscripts s and d refer to the sum and difference, respectively. The discrete time all-pass functions are defined by

$$A_1(z)\equiv\frac{D_1^R(z)}{D_1(z)} \quad \text{and} \quad A_2(z)\equiv\frac{D_2^R(z)}{D_2(z)} \quad (6)$$

where the denominator polynomial in (5) is given by $D(z)=D_1(z)D_2(z)$. The numerator polynomials $N_s(z)$ and $N_d(z)$ were previously assumed [2] to have either even or odd symmetry and real coefficients. We now allow the coefficients to be complex so that multiple passbands can be obtained and arbitrary magnitude responses approximated. By introducing the new phase term θ which is discussed below, the decomposition into all-pass functions is generalized as follows:

$$H_s(z)=\tfrac{1}{2}[A_1(z)+A_2(z)] \quad (7)$$

$$H_d(z)=\frac{e^{-j\theta}}{2}[A_1(z)-A_2(z)]. \quad (8)$$

Given a lossless filter with two outputs and a desired $H_s(\omega)$ response, the $H_d(\omega)$ magnitude response can be found from power conservation

$$|H_s(\omega)|^2+|H_d(\omega)|^2=1. \quad (9)$$

For an optical filter, any lossless 2×2 splitter (and combiner, by reciprocity) has a $\pi/2$ relative phase between the output ports [10] that must be included. For a directional coupler, let the cross-port field transmission be denoted by $-j\sqrt{\kappa}$ and the bar-port by $\sqrt{1-\kappa}$. Ideally, the couplers forming the MZI have $\kappa=0.5$. The optical transfer functions, designated by the bar and cross-ports of the interferometer, are

$$H_{-}(z)=\tfrac{1}{2}[A_1(z)-A_2(z)] \quad (10)$$

$$H_x(z)=\frac{-j}{2}[A_1(z)+A_2(z)]. \quad (11)$$

Note that the magnitude responses of the discrete time and optical filters are related by $|H_s(\omega)|^2=|H_x(\omega)|^2$ and $|H_d(\omega)|^2=|H_{-}(\omega)|^2$, so that the phase difference between (8) and (10), or (7) and (11), is inconsequential.

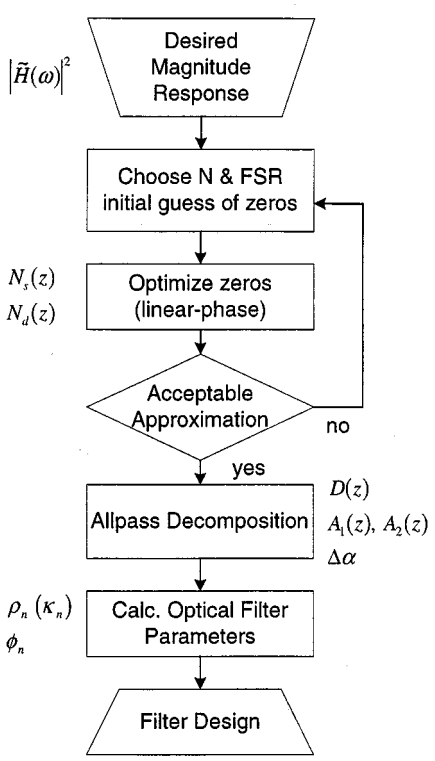

Fig. 3. General optical IIR filter synthesis algorithm using all-pass filter decomposition.

The general synthesis algorithm is outlined in Fig. 3. The input is the desired magnitude response $|\tilde{H}(\omega)|^2$ specified over some optical bandwidth. The outputs are the parameters (ρ_n's and ϕ_n's) that define a specific optical implementation. The FSR is set equal to or slightly larger than the bandwidth, and the number of filter stages is specified. The optical frequency f is normalized to the FSR, so the desired response is specified as a function of the normalized frequency $v=f/\text{FSR}$ where $0\le v<1$, and the design algorithm proceeds in the digital domain. Depending on the desired "goodness" of the approximation, more stages may be required. The intervening steps start with an initial digital design guess, refine that guess until an acceptable approximation is obtained, decompose the transfer functions into all-pass filters, and then translate the discrete time all-pass filter designs into optical ones.

Several approaches can be used to obtain an initial guess at a discrete time filter design. Examples are given in later sections dealing with specific designs. A simple way to determine $H_s(z)$ and $H_d(z)$, especially for bandpass filters, is by finding suitable zeros. For now, we assume that the zeros of $N_s(z)$ and $N_d(z)$ are defined. If we multiply (9) by $|D(\omega)|^2$ and divide by $|N_s(\omega)|^2$, we obtain [11]

$$1+\frac{|N_d(\omega)|^2}{|N_s(\omega)|^2}=\frac{|D(\omega)|^2}{|N_s(\omega)|^2}=\frac{1}{|H_s(\omega)|^2}. \quad (12)$$

In the Z-domain, $K(z)=N_d(z)/N_s(z)$ is called the characteristic function. By evaluating $K(z)$ on the unit circle, the magnitude response $|H_s(\omega)|^2$ is defined. Similarly, dividing by

$|N_d(\omega)|^2$ instead of $|N_s(\omega)|^2$, the magnitude response $|H_d(\omega)|^2$ is obtained. The characteristic function for $H_d(\omega)$ is $1/K(z)$. Thus, the characteristic function, which is defined solely by the zeros of the numerator polynomials, defines the magnitude responses for both $H_s(\omega)$ and $H_d(\omega)$.

The next step is to find $D(z)$, and then $A_1(z)$ and $A_2(z)$. It is important to note that only the magnitudes of $H_s(\omega)$ and $H_d(\omega)$ are determined by (12), leaving a constant phase for each response undetermined. Since only the relative phase is important, let θ represent the phase difference so that the all-pass functions are now defined as follows:

$$A_1(z) = H_s(z) + e^{j\theta} H_d(z)$$

and

$$A_2(z) = H_s(z) - e^{j\theta} H_d(z). \tag{13}$$

From [5], we know that if $N_2(z)$ has odd order and symmetry, $\theta = 0$. If it has even order and symmetry, then $\theta = \pi/2$. For the general case, we must determine θ. Setting $|A_1(\omega)| = |A_2(\omega)| = 1$ at an arbitrary frequency, say $z = 1$, results in $|N_s(1) + e^{j\theta} N_d(1)| = |N_s(1)| - e^{j\theta} N_d(1)$. Let the phase of $N_s(1)$ and $N_d(1)$ be represented by η_s and η_d, then θ is given by

$$\theta = \eta_s - \eta_d + \frac{\pi}{2}(2m+1) \tag{14}$$

where m is an integer. Equation (14) is equivalent to the condition for the phases of any 2×2, lossless device whose transmission can be described by a unitary matrix [10]. The roots of the denominator polynomials can now be determined by multiplying the relationships in (7), (8) by $D(z)$ to obtain

$$N_s(z) + e^{j\theta} N_d(z) = D_1^R(z) D_2(z) \tag{15}$$

$$N_s(z) - e^{j\theta} N_d(z) = D_1(z) D_2^R(z). \tag{16}$$

For (15), the minimum-phase roots of the left-hand side ($|p_n| < 1$) are used to define $D_2(z)$ and the maximum-phase roots ($|p_n| > 1$) to define $D_1^R(z)$. A scale factor is then determined for $N_s(z)$ and $N_d(z)$ to satisfy (9). The denominator of $A_1(z)$ and $A_2(z)$ are fully defined as well as the roots of the numerators. There is, however, a constant phase α associated with each all-pass filter that must be determined. The phase is found by evaluating (13) at a particular frequency, for example $z = 1$

$$e^{j\alpha_1} A_1(1) = e^{j\alpha_1} \frac{D_1^R(1)}{D_1(1)} = \frac{N_s(1)}{D(1)} + e^{j\theta} \frac{N_d(1)}{D(1)} \tag{17}$$

$$e^{j\alpha_2} A_2(1) = e^{j\alpha_2} \frac{D_2^R(1)}{D_2(1)} = \frac{N_s(1)}{D(1)} - e^{j\theta} \frac{N_d(1)}{D(1)}. \tag{18}$$

The design parameters for an optical ring (or cavity) implementation are obtained from the discrete time all-pass responses. The relative phase between the MZI arms is $\Delta\alpha = \alpha_1 - \alpha_2$. The coupling (or reflection strengths for the cavity design) and phases for each all-pass filter are then determined as discussed in [2]. For a simple cascade of rings, as shown in Fig. 1(c), the roots of $D_1(z)$ and $D_2(z)$ are related to the optical parameters by $\kappa_n = 1 - |p_n|^2$ and $\phi_n = \arg(p_n)$. The total phase from the extra phase term in (2) for an optical all-pass filter must be compensated by adding $\phi_{\text{tot}} = -\Sigma_{n=1}^{N} \phi_n$ to each arm.

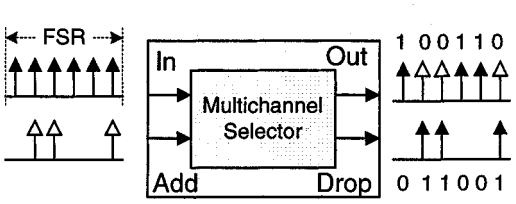

Fig. 4. Schematic of a multichannel frequency selector for add and drop, and the corresponding binary representation of the drop and through states.

The conditions on $H_s(z)$ and $H_d(z)$ required for all-pass decomposition can be understood by expressing the numerator polynomials as follows:

$$N_s(z) = [D_1^R(z) D_2(z) + D_1(z) D_2^R(z)]/2 \tag{19}$$

$$N_d(z) = e^{-j\theta} [D_1^R(z) D_2(z) - D_1(z) D_2^R(z)]/2. \tag{20}$$

By defining the reverse polynomials, it is easily shown that $N_s(z) = N_s^R(z)$ and $N_d(z) = -e^{-2j\theta} N_d^R(z)$; thus, the numerator polynomials are linear-phase [10]. Linear-phase polynomials have their roots on the unit circle ($|z_n| = 1$) or have pairs of roots located reciprocally about the unit circle $(z_n, 1/z_n^*)$. The denominator polynomial must be minimimum-phase (all $|\rho_n| < 1$) for a stable, causal filter.

III. Multichannel Frequency Selector

A multichannel frequency selector drops (or adds) any of N incoming channels while passing the remaining channels through the device as illustrated in Fig. 4. For a given output port, each channel is either on or off, which can be represented by a "1" or "0." The other output has the complementary response by power conservation. Add/drop filters must satisfy strict requirements on the passband flatness so that many filters can be cascaded in the system without reducing the passband width. In addition, the filters must meet tight requirements on crosstalk. The crosstalk may result from leakage of adjacent or nonadjacent channels into the output for a particular channel. A greater concern is leakage of a dropped channel into the through path that may interfere with an added channel at the same wavelength later in the system. A periodic filter capable of selecting multiple channels within one FSR that are not necessarily adjacent is discussed. The multichannel frequency selector concept was first proposed and demonstrated for an eight channel selector using a transversal FIR filter structure [12]. The major drawback was the achievable crosstalk for a given number of filter stages and channels. More recently, single-passband lattice FIR filters have been demonstrated [13], [14], capable of operating on four channels per FSR.

The synthesis algorithm is now used to design a multiple passband filter so that several wavelengths, not necessarily adjacent, can be selected per FSR for adding or dropping in a similar fashion to the FIR frequency selector of [12]. As an example, a 12th-order filter was designed to drop channels 1 and 4 out of eight channels equally spaced across the FSR. Since 100%

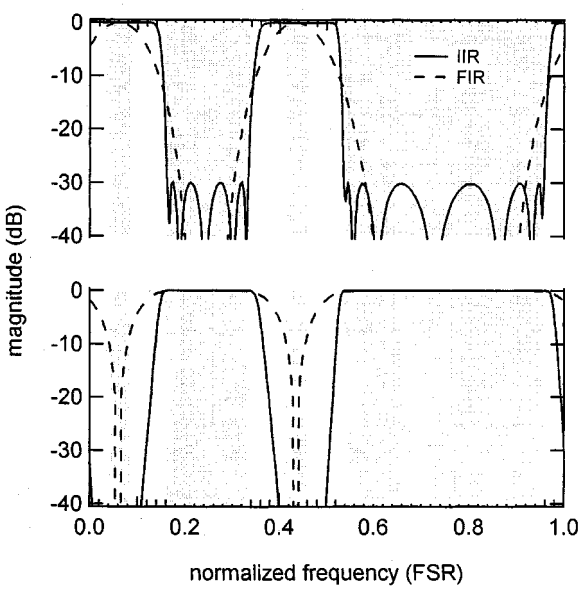

Fig. 5. Power complementary responses for a 12th-order, eight-channel IIR (solid) and FIR (dashed) frequency selector for the (top) [1 0 0 1 0 0 0 0] and (bottom) [0 1 1 0 1 1 1 1] states.

TABLE I
DESIGN PARAMETERS FOR A 12TH-ORDER IIR MULTICHANNEL FREQUENCY SELECTOR FOR STATE [1 0 0 1 0 0 0 0]. THE RELATIVE PHASES ARE $\theta = 3.585$, $\alpha 1 = -2.962$, AND $\alpha 2 = -2.964$ RADIANS

n	κ_{n1}	ϕ_{n1}	κ_{n2}	ϕ_{n2}
1	0.136	0.926	0.100	-2.976
2	0.164	2.213	0.123	-0.174
3	0.320	-2.929	0.421	0.997
4	0.388	-0.227	0.500	2.125
5	0.805	1.332	0.628	-2.842
6	0.980	-2.927	0.734	-0.317

transmission is desired for the passband frequencies of one response, the zeros of the opposite response were located on the unit circle across the respective stopbands for an initial guess. Locating the zeros on the unit circle produces linear-phase numerator polynomials as required for the all-pass decomposition. The solution was refined by numerical optimization in a least squares sense to yield the spectral responses shown in Fig. 5. For comparison, the response for a 12th-order FIR filter was optimized in a similar fashion. The target was to achieve a 30-dB stopband rejection over a channel width equal to 40% of the channel spacing. The stopband was extended between adjacent off-channels. A slightly better stopband rejection and passband width can be obtained by localizing the stopband around each channel. The stopbands used in the optimization are indicated by the shaded regions. The IIR selector meets the design requirements for both responses. The IIR response decomposes into two, sixth-order all-pass filters. The coupling ratios and phases for each all-pass filter are listed in Table I. All of the coupling ratios are distinct and fall within a reasonable fabrication range, $0.1 \leq \kappa \leq 0.98$. The FIR filter offers good rejection over a localized frequency region but fails to meet the specified design requirements for either response. Tradeoffs can be made between the passband flatness and stopband rejection for

TABLE II
UNIQUE STATES DEPENDING ON THE NUMBER OF CHANNELS (N) PER FSR WHERE CHANNEL ON = 1 AND OFF = 0. THE NULL STATE (ALL CHANNELS ON OR OFF) WAS EXCLUDED

N=2 (1 state)				
1	0			
N=3 (1 state)				
1	0	0		
N=4 (3 states)				
1	0	0	0	
1	1	0	0	
1	0	1	0	
N=5 (3 states)				
1	0	0	0	0
1	1	0	0	0
1	0	1	0	0

FIR filters. Separate multistage filters may be required to obtain both, as demonstrated in [13] where a seven-stage filter with good passband flatness on the drop channels was cascaded with a five-stage filter to improve the add-to-drop channel isolation. We note that other design approaches have been investigated for discrete time multiband filters [15].

A versatile multichannel selection filter can be configured to drop any channel or number of channels. The number of different filter states that must be generated and satisfy the design requirements (passband width, stopband rejection, etc.) depends on the number of channels per FSR. For N channels, there are 2^N possible states; however, it is only necessary to consider a subset. The remaining states can be obtained by the following transformations: 1) the power complementary response is obtained by changing the phase between the arms of the MZI by π; 2) the response is translated in frequency by changing all of the phases by a fixed amount; or 3) the response is reversed by conjugating the filter parameters. Table II lists the unique states as a function of the number of channels. The null state, consisting of all channels on or off, was not included. The null state can be achieved by changing the MZI coupling ratios to "0" or "1" so that the input goes into one arm of the interferometer. For $N = 8$, there are 18 unique states (including the null state) compared to 256 total states, thus the design space that must be optimized and the complexity of the control algorithm are substantially reduced. All states for the $N = 4$ case can be obtained from three, symmetric responses. For higher channel counts per FSR, nonsymmetric cases must be realized for a completely versatile selector. The advantage of symmetric states is that the symmetry is also present in the all-pass decomposition, so fewer unique coupling ratios and phases have to be realized. For example, the design parameters for the three states of the $N = 4$ case are given in Table III for an eighth-order response. Each state decomposes into fourth-order all-pass filters in each arm. The coupling ratios are identical for $A_1(z)$ and $A_2(z)$, while the phases are opposite in sign. The corresponding spectra are shown in Fig. 6. The design requirements are met with margin for all states. For a reconfigurable multichannel selector, it is important that all of the states decompose into all-pass filters of the same order in each arm. We note that a sixth-order filter meets the above design requirements on stopband rejection and passband width; however, the [1 0 1 0] state decomposes into a fourth-order and second-order all-pass filter. Thus, a filter with

TABLE III
DESIGN PARAMETERS FOR AN EIGHTH-ORDER IIR MULTICHANNEL FREQUENCY SELECTOR FOR STATES $s1$ = [1 0 0 0], $s3$ = [1 1 0 0], and $s5$ = [1 0 1 0]. NOTE THAT $\phi_{n1} = -\phi_{n2}$ AND $\kappa_{n1} = \kappa_{n2}$

Coupling Ratios (κ_n)			Phase (ϕ_{n1} radians)		
s1	s3	s5	s1	s3	s5
0.786	0.934	0.726	-0.483	-1.698	-0.800
0.454	0.568	0.726	0.787	1.637	2.341
0.187	0.245	0.238	-0.825	-1.633	0.793
0.048	0.065	0.238	0.829	1.632	-2.348
MZI Phase					
Δα1	Δα3	Δα5			
-1.154	-0.755	-0.778			

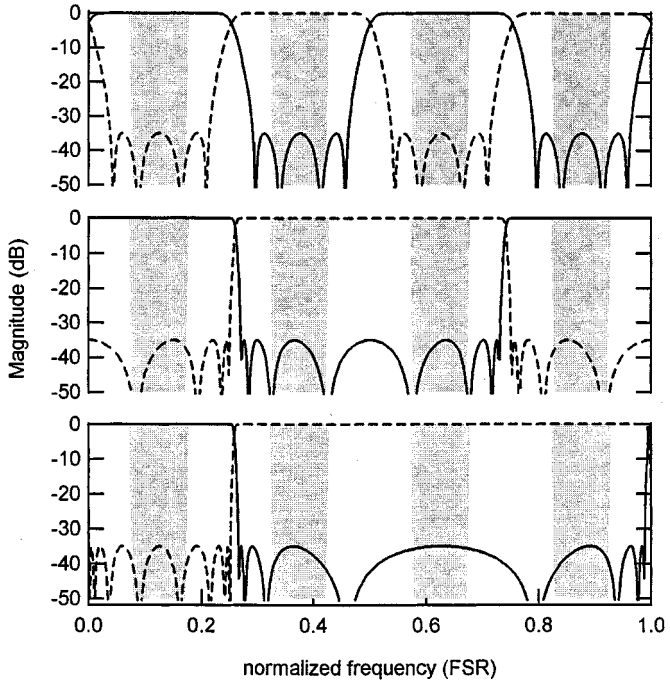

Fig. 6. Output spectra for three states of an eighth-order, four-channel IIR frequency selector.

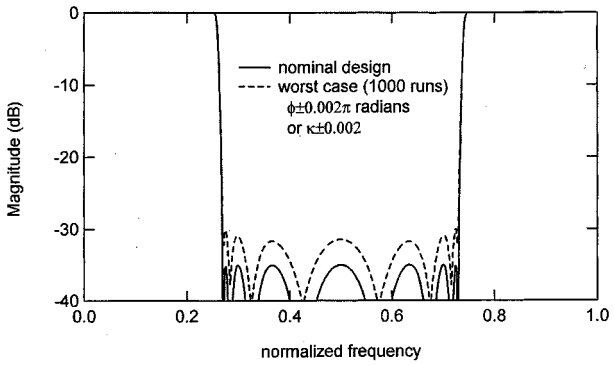

Fig. 7. Worst case spectra of 1000 runs for uniformly varying random phase and coupling ratio on an eighth-order, four-channel IIR frequency selector response.

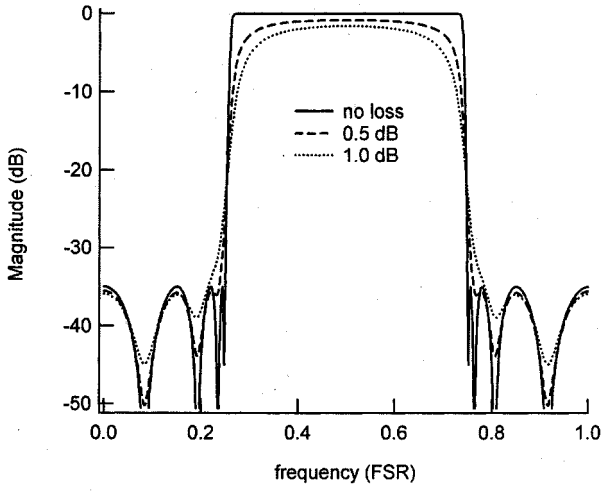

Fig. 8. Impact of loss on an eighth-order, four-channel IIR frequency selector response.

a three-stage all-pass filter in each arm would not be able to realize this response.

Next, we explore the design sensitivity to variations in the coupling ratios, loss and phases using the nominal all-pass filter designs for state $s3$ from Table III in (10), (11) as the starting point. To maintain a stopband rejection of 30 dB on an eight-stage filter with a nominal 35 dB rejection, the coupling ratios must be within ± 0.002 and the phases within $\pm 0.002\pi$. The worst case stopband rejection over 1000 runs, assuming a uniform distribution on the coupling ratios and phases, is shown in Fig. 7. For a four-stage filter with a minimum 30 dB rejection, the coupling tolerance is ± 0.003 and the phase tolerance is $\pm 0.005\pi$ The lower-order filter is substantially more tolerant to phase errors. Waveguide heaters have demonstrated phase tolerances better than $\pm 0.01\pi$ [16]. The impact of a 0.5- and 1.0-dB loss per feedback path is shown in Fig. 8. The passband transmission decreases proportional to the feedback path loss, but the stopband response is maintained. The tolerance to loss results because the passband and stopband occur off-resonance for the all-pass filters. Feedback path losses of 1 dB have been achieved in practice [17], and lower losses are anticipated. For a 30-dB stopband rejection, the coupling ratios of the MZI must be tightly controlled, $\kappa = 0.500 \pm 0.016$. In practice, each coupler may be realized with a symmetric MZI having a phase shifter in one arm to tune the effective coupling ratio.

As a specific example, consider a filter with a 100-GHz FSR designed to separate channels spaced on a 25 GHz grid. For a waveguide effective index of $n_g = 1.5$, the nominal feedback path length is $L = 2$ mm. Next, we consider the tolerances on the coupling ratios and phases for operation over a wavelength range of $\Delta\lambda$. An added benefit byproduct of using MZI's to implement tunable couplers is that the effective coupling wavelength dependence can be made negligible, for example $\kappa = 0.200 \pm 0.005$ over 100 nm [18]. The nominal phases are set using heaters, so we need only consider the wavelength dependent phase error. Let $\Delta\phi \equiv |d\phi/d\lambda|\Delta\lambda \leq 0.001\pi$, then the tolerance on the feedback path length is $\Delta(nL) \leq 5 \times 10^{-4}(\lambda^2/\Delta\lambda)$. For $\lambda = 1550$ nm and $\Delta\lambda = 30$ nm, $\Delta(nL) = 0.04$ μm which is commensurate with tolerances for waveguide grating routers [19].

IV. Filters with Arbitrary Magnitude Responses

The all-pass filter decomposition architecture is not limited to bandpass designs. A simple modification of the bandpass design is to replace the 3-dB couplers in the MZI with other values. The square magnitude response depends on the coupling ratios and all-pass filter phase responses as follows:

$$|H_x(\omega)|^2 = 4\kappa(1-\kappa)\cos^2\left(\frac{\Phi_1(\omega)-\Phi_2(\omega)}{2}\right) \qquad (21)$$

where $A_{1,2}(\omega) = e^{j\Phi_{1,2}(\omega)}$. For example, let the coupling ratios be given by κ = 0.3 (5.2 dB) and assume that each arm has a four-stage all-pass filter designed for an eighth-order elliptic filter response. The spectral response shape can be made the same as shown in Fig. 6, except that $|H_x(\omega)|^2$ has a maximum equal to -0.8 dB while its power complementary response has a minimum of -8 dB. Thus, each spectral response has two levels that can be varied by choosing the splitting and combining coupling ratios of the MZI.

Now, we consider the design of a filter with an arbitrary IIR spectral response using all-pass decomposition. The problem is to determine $A_1(z)$ and $A_2(z)$ so that one of the filter responses closely approximates the desired square magnitude response, $|\tilde{H}(\omega)|^2$. The filter order is equal to the sum of the number of stages in $A_1(z)$ and $A_2(z)$. If the desired response fluctuates between two levels, a bandpass filter design approach can be used with the MZI coupling ratios chosen using (21) and power conservation for the other response. For more general filter functions, the characteristic function approach is used to set the zeros for the numerator polynomials, $N_s(z)$ and $N_d(z)$. The numerator polynomials must be linear-phase so that (17) and (18) are satisfied for the same value of θ. In general, setting the zeros for any two of the three polynomials (N_s, N_d or D) defines the zeros for the remaining polynomial as a result of the power conservation relationship extended analytically to the Z domain [10], the linear-phase condition on $N_s(z)$ and $N_d(z)$, and the stability requirement on $D(z)$.

A. Linear Power Response

As an example, a filter with a linear square magnitude response over $0.15 \le v \le 0.85$ was designed. Only frequencies within this range were used in the numerical optimization. The square magnitude response for a second-order filter is shown in Fig. 9. The response is linear to within ± 0.005 over a frequency range of 0.64 $\times$ FSR. By comparison, an asymmetric MZI response has an approximately linear response over a much narrower range of the FSR. The IIR filter contains a single-stage all-pass filter in each arm of the MZI. The pole magnitudes and phases (rad) for the all-pass filters are $0.2925 \angle 0.0088$ and $0.7865 \angle -0.0099$. The remaining design parameters are $\kappa = 0.5, \theta = -0.7121$, and $\Delta\alpha = -1.5896$ radians. Potential applications for such a response include frequency discriminators for laser wavelength tracking and stabilization and modulators that respond linearly to the input signal for analog transmission.

B. Gain Equalization Filter

Next, we design an IIR filter to approximate a desired gain equalization function to within 0.1 dB. The desired response is taken from a 20-nm portion of an erbium-doped fiber amplifier spectrum. For a starting point, the output of an all-pole (or autoregressive filter) model [10] is used for the pole locations, and the zeros are set at $z_n = 0$. An optimization routine is then used to find the best fit in a least squares sense for a given order IIR response. The shortest IIR filter amenable to all-pass decomposition to meet the above criterion is fourth-order. The magnitude response is shown in Fig. 10, and the filter design values are given in Table IV. To avoid large coupling ratios ($\kappa > 0.99$), the

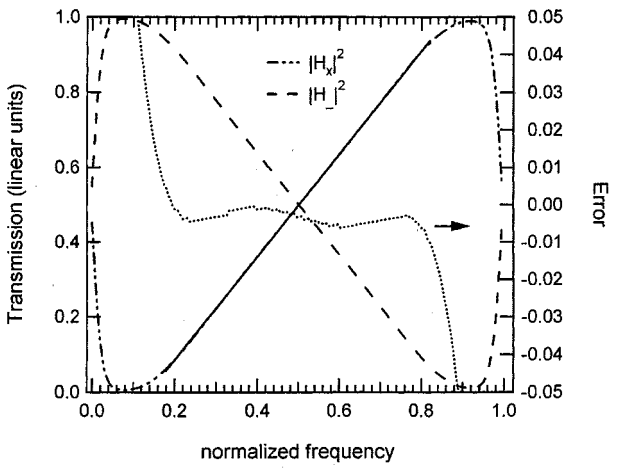

Fig. 9. Linear power response for an IIR filter with a single-stage all-pass filter in each arm of a MZI.

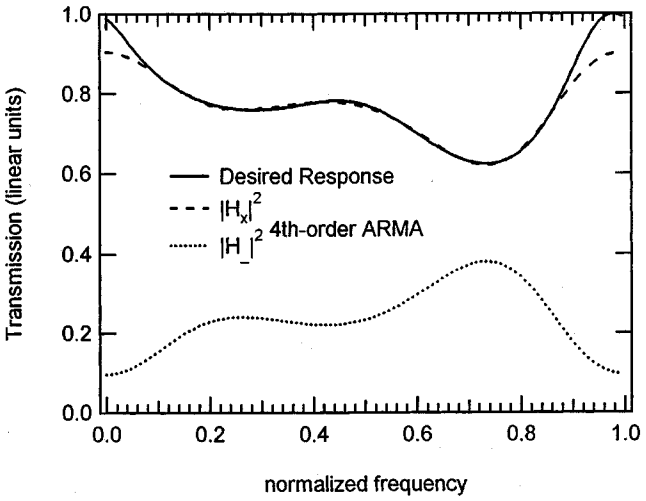

Fig. 10. Gain equalization filter response.

TABLE IV
Design Parameters for a Fourth-Order Gain Equalization IIR Filter

	$A_1(z)$		$A_2(z)$	
n	κ_{n1}	ϕ_{n1}	κ_{n2}	ϕ_{n2}
1	0.928	-2.408	0.779	-0.333
2	0.791	0.003	0.970	-2.471
θ	α_1		α_2	
1.172	-0.246		-0.798	

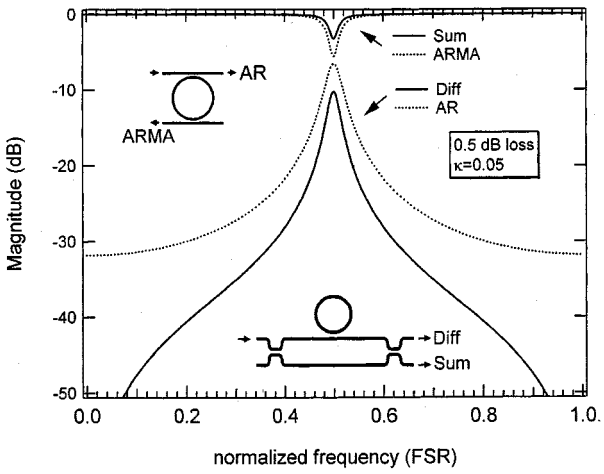

Fig. 11. Notch filter response compared to a single-ring filter response.

peak filter transmission was reduced from 100% to 89% (0.5 dB loss). The combination of poles and zeros in one filter allows a lower order filter (thus a simpler and potentially more compact implementation) to be used to meet the same requirements of an all-zero or all-pole filter. For a lossy filter, the loss changes the spectral shape, so it is necessary to include the loss as part of the design optimization. Similar design parameters and fit were obtained for the above IIR filter by optimizing for a 0.5 dB loss per feedback path round-trip.

V. Special Case: A Delay Line in One Arm

We now consider IIR filters using all-pass decomposition where one arm is a simple delay line. Two examples with potential applications for WDM systems are given: a notch filter and a multistep response filter.

A. A Notch Filter

A notch filter removes a single frequency in the FSR. Such a response can be achieved by using a single-stage all-pass filter in one arm of a MZI and a delay in the other arm as indicated in the inset of Fig. 11. Both arms have the same delay if $\kappa = 0$ for the all-pass filter. Multiple notches per FSR can also be used by adding more all-pass stages [20]. By varying the ring coupling ratio, the finesse of the response changes. The response is very similar to a single-pole, or autoregressive (AR), response obtained from a ring with two couplers; however, it has a zero in the transfer function that improves the stopband rejection. The notch filter is compared to a ring resonator response in Fig. 11 assuming the coupling to the ring is $\kappa = 0.05$ in both cases and that the loss per round-trip for the feedback path is 0.5 dB. The through-path response for the ring has a single pole and zero, making it an IIR or moving-average autoregressive (ARMA) response. If there were no loss, then the power complementary responses would have a notch with zero transmission. With loss, however, the notch depth is substantially reduced in both cases. As the finesse increases, the peak transmission decreases for both filters in the presence of loss. The peak transmission is -6.8 and -10.6 dB for the AR and notch filter responses, respectively.

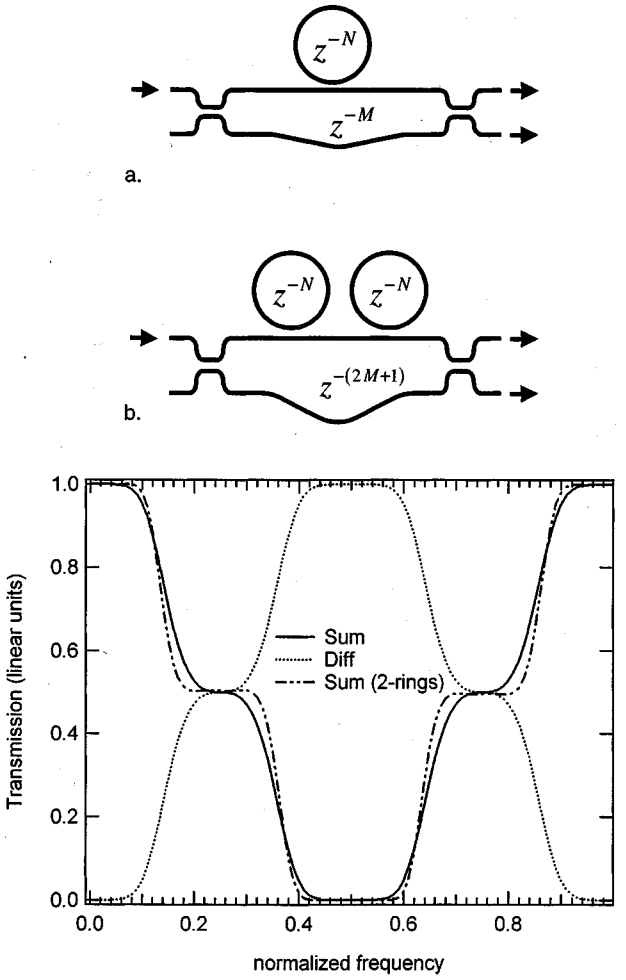

Fig. 12. Multistep architecture and response for (a) a single-stage and (b) double-stage all-pass filter with $N = 4$ and $M = N - 1$.

B. A Multistep Filter

A multistep response is easily obtained using all-pass filters in one arm and a delay in the other arm. Let the all-pass filter delay be z^{-N} and the delay line be z^{-M}. Over one FSR, the all-pass filter goes through N periods and has a total phase change of $-2\pi N$, while the delay line phase changes linearly by $-2\pi M$. By choosing the phase slope (i.e., group delay) of the all-pass filter equal to that of the delay line over some portion of its period, the magnitude response of the MZI stays constant over that region. Furthermore, choosing $M = N - 1$ means that the phase difference between the arms after one FSR is 2π and that the delay line is shorter than the all-pass filter feedback path. The off-resonance group delay $(\tau_{\min})$ of the all-pass filter is then set equal to the group delay of the delay line by choosing ρ according to (4). For a single ring with $M = 3$ and $N = 4$, a three-level response results as shown in Fig. 12. The ring coupling is ρ = 0.1429. By adding another all-pass filter stage, the width of each step can be increased while decreasing the transition band. The response using a two-stage all-pass filter in one MZI arm and lengthening the delay line so that $M = 2N - 1$ is also shown in Fig. 12. The two-stage all-pass filter was optimized for constant delay over 0.6 $\times$ FSR and has the design

parameters $\rho_1 = 0.1493 \angle 3.1102$ and $\rho_2 = 0.3721 \angle 6.2517$. The architecture is advantageous for ring implementations since a larger ring diameter, proportional to N/FSR instead of 1/FSR, is required. This same design approach can be used to extend the passband width of a multiport filter incorporating all-pass filters [21]. Larger values of N (with $M = N - 1$) increase the number of levels in the response. Discrete time arbitrary-level filters are discussed in [22], [23].

VI. Discussion

In summary, an all-pass filter decomposition algorithm was defined for the design of multiple-passband filters. The previous single-passband algorithm was modified by introducing two phase terms, θ and $\Delta\alpha$, and the characteristic function. The resulting IIR multichannel frequency selector has substantially better passband flatness and stopband rejection than is possible with an FIR filter having the same number of stages. Architectures using all-pass filters can also be used to realize arbitrary functions such as those required for gain equalization, linear, and multistep responses. While these structures are quite tolerant to loss, good control over the coupling and phases is required just as for FIR filters like the waveguide grating router. Reconfigurable IIR filters can be realized using tunable all-pass filters as building blocks.

The filter theory presented is general and can be implemented in many different technology platforms. While ring implementations in planar waveguides are attractive from a compact device and integration viewpoint, they require high core-to-caldding index contrasts to obtain the ring radii required for some applications. Demonstrations of microcavity rings [24], [25] show that FSR's suitable for multichannel filter applications in WDM systems are achievable. Coupling from a low to high index contrast waveguide must be addressed as well as minimizing polarization dependence. These challenges must also be addressed for photonic bandgap (PBG) structures. PBG structures provide an opportunity for integrated, standing-wave cavity all-pass filters using partially reflecting Bragg gratings instead of couplers. The challenge for standing-wave cavity filters is to fabricate the desired partial reflectance with a small wavelength dependence, to separate the incoming and reflected signal, and to realize cascaded or coupled cavities. Besides planar integration, the architectures discussed in this paper can be implemented using optical MEM's devices [8] and thin film filters [26].

References

[1] K. Harada, K. Shimizu, T. Kudou, and T. Ozeki, "Hierarchical optical path cross-connect systems for large scale WDM networks," in *Proc. Optical Fiber Commun. Conf.: Int. Conf. Integr. Optics and Optical Fiber Commun.*, San Diego, CA, Feb. 2–26, 1999, Paper WM55.

[2] C. Madsen, "Efficient architectures for exactly realizing optical filters with optimum bandpass designs," *IEEE Photon. Technol. Lett.*, vol. 10, pp. 1136–1138, Aug. 1998.

[3] R. Ansari and B. Liu, "A class of low-noise computationally efficient recursive digital filters with applications to sampling rate alterations," *IEEE Trans. Acoust., Speech, Signal Processing*, vol. 33, pp. 90–97, Jan. 1985.

[4] C. Madsen and G. Lenz, "Optical allpass filters for phase response design with applications for dispersion compensation," *IEEE Photon. Technol. Lett.*, vol. 10, pp. 994–996, July 1998.

[5] F. Gires and P. Tournois, "Interferometer utilisable pour la compression d'impulsions lumineuses modulees en frequence," *C. R. Acad. Sci.*, vol. 258, no. 5, pp. 6112–6115, 1964.

[6] L. Soldano and E. Pennings, "Optical multi-mode interference devices based on self-imaging: Principles and applications," *J. Lightwave Technol.*, vol. 13, pp. 615–627, Apr. 1995.

[7] C. Madsen, "An infinite impulse response multichannel frequency selector," in *Proc. Integr. Photon. Res.*, Santa Barbara, CA, July 1999, Paper RTuA4.

[8] C. Madsen, J. Walker, J. Ford, K. Goossen, and G. Lenz, "A tunable dispersion compensating MARS all-pass filter," in *Proc. Eur.Conf. Optic. Commun.*, Nice, France, 1999.

[9] G. Lenz and C. Madsen, "General optical all-pass filter structures for dispersion control in WDM systems," *J. Lightwave Technol.*, vol. 17, pp. 1248–1254, July 1999.

[10] C. Madsen and J. Zhao, *Optical Filter Design and Analysis: A Signal Processing Approach*. New York: Wiley, 1999.

[11] A. Willson and H. Orchard, "Insights into digital filters made as the sum of two allpass functions," *IEEE Trans. Circuits Syst.*, vol. 42, no. 3, pp. 129–137, 1995.

[12] K. Sasayama, M. Okuno, and K. Habara, "Photonic FDM multichannel selector using coherent optical transversal filter," *J. Lightwave Technol.*, vol. 12, pp. 664–669, Apr. 1994.

[13] R. Germann, R. Beyeler, G. Bona, F. Horst, B. Offrein, and H. Salemink, "Tunable optical add/drop components in silicon-oxynitride waveguide structures," in *Proc. Optic. Fiber Commun. Conf. Int. Conf. Integr.Opt. Optic. Fiber Commun.*, San Diego, CA, Feb. 23–26, 1999, Paper WM25.

[14] B. Offrein, R. Germann, G. Bona, F. Horst, and H. Salemink, "Tunable optical add/drop components in silicon-oxynitride waveguide structures," in *Proc. 24th Eur. Conf. Opt. Commun. (ECOC)*, Madrid, Spain, Sept. 20–24, 1998, pp. 325–326.

[15] S. Pei and J. Shyu, "Design of IIR multiband filters using IIR all-pass filters," *Signal Processing*, vol. 37, pp. 87–94, 1994.

[16] N. Takato, K. Jinguji, M. Yasu, H. Toba, and M. Kawachi, "Silica-based single-mode waveguides on silicon and their application to guided-wave optical interferometers," *J. Lightwave Technol.*, vol. 6, no. 6, pp. 1003–1010, 1988.

[17] C. K. Madsen, G. Lenz, A. J. Bruce, M. A. Cappuzzo, L. T. Gomez, and R. E. Scotti, "Integrated all-pass filters for tunable dispersion and dispersion slope compensation," *IEEE Photon. Technol. Lett.*, vol. 11, no. 12, pp. 1623–1625.

[18] K. Jinguji, N. Takato, A. Sugita, and M. Kawachi, "Mach-Zehnder interferometer type optical waveguide coupler with wavelength-flattened coupling ratio," *Electron. Lett.*, vol. 16, no. 17, pp. 1326–1327, 1990.

[19] Y. P. Li and C. H. Henry, "Silicon optical bench waveguide technology," in *Optical Fiber Telecommunications IIIB*. New York: Academic , 1997, pp. 319–376.

[20] S. Pei and C. Tseng, "IIR multiple notch filter design based on allpass filter," *IEEE Trans. Circuits Syst. II*, vol. 44, no. 2, pp. 133–136, 1997.

[21] C. Madsen, "A multiport band selector with inherently low loss, flat passbands and low crosstalk," *IEEE Photon. Technol. Lett.*, vol. 10, no. 12, pp. 1766–1768, 1998.

[22] R. Ansari, "Multi-level IIR digital filters," *IEEE Trans. Circuits Syst.*, vol. CAS-33, pp. 337–341, Mar. 1986.

[23] R. Koilpillai, P. Vaidyanathan, and S. Mitra, "On arbitrary-level IIR and FIR filters," *IEEE Trans. Circuits Syst.*, vol. 37, no. 2, pp. 280–284, 1990.

[24] J. Foresi, B. Little, G. Steinmeyer, E. Thoen, S. Chu, H. Haus, E. Ippen, L. Kimerling, and W. Greene, "Si/SiO_2 micro-ring resonator optical add/drop filters," in *Proc. CLEO Conf.*, Baltimore, MD, May 18–23, 1997, Paper CPD22-2.

[25] D. Rafizadeh, J. Zhang, S. Hagness, A. Taflove, K. Stair, and S. Ho, "Nanofabricated waveguide-coupled 1.5-μm microcavity ring and disk resonators with high Q and 21.6-nm free spectral range," in *Proc. CLEO Conf.*, Baltimore, MD, May 18–23, 1997, Paper CPD23-2.

[26] C. K. Madsen and G. Lenz, "A multi-channel dispersion slope compensating optical allpass filter," in *Proc. Optic. Fiber Conf.*, Baltimore, MD, Mar. 5–10, 2000, Paper WF5.

C. K. Madsen, photograph and biography not available at the time of publication.